Supporting Information for

Electronic structure engineering of heterogeneous ceria-incorporated Pt/C as an efficient catalyst for boosting DMFCs performance

Ziqi Wan[a,b], Jianqi Ye[a], Jinyuan Zhang[a], Jie Gao[c], Lei Liu[d,*], Dan Wen [a,*] and Wei Gao[a,b,*]

[a] *State Key Laboratory of Solidification Processing, School of Materials Science and Engineering, Northwestern Polytechnical University, Xi'an, 710072, P. R. China*

[b] *Chongqing Innovation Center, Northwestern Polytechnical University, Chongqing, 401135, P. R. China*

[c] *School of Life Sciences, Northwestern Polytechnical University, Xi'an, 710072 P. R. China*

[d] *National Clinical Research Center for Digestive Diseases and State Key Laboratory of Holistic Integrative Management of Gastrointestinal Cancers, Xijing Hospital of Digestive Diseases, Fourth Military Medical University, Xi'an 710032, China.*

* Corresponding authors should be addressed to: liulei84207@163.com (L. Liu), dan.wen@nwpu.edu.cn (D. Wen), and wei.gao@nwpu.edu.cn (W. Gao).

Experimental section

1. Chemicals and Reagents

Cerium chloride heptahydrate ($CeCl_3 \cdot 3H_2O$, 99%) and Nafion solution (5 wt%) were obtained from Alfa Aesar. Potassium hydroxide (KOH, 95%) and methanol (CH_3OH, AR) were sourced from Aladdin chemical reagent. 20 % JM Pt/C was procured from Shanghai Hesen Electric Co., Ltd. 20 % PtRu/C was acquire from Accelerate®. Acetonitrile (C_2H_3N, AR), and perchloric acid ($HClO_4$, AR) were acquired from Sinopharm chemical reagent company. All chemicals were used as received, without further purification. The aqueous solutions were prepared with deionized water with a resistivity of 18.2 MΩ·cm.

2. Synthesis of Pt-CeO_2/C heterogeneous catalyst

The Pt-CeO_2/C heterogeneous catalyst was synthesized through the wet impregnation method, utilizing Pt/C and $CeCl_3$ as the precursor materials. The Pt-CeO_2/C heterogeneous catalyst was synthesized by the wet impregnation method using Pt/C and $CeCl_3$ as precursors. Typically, Pt/C (25 mg) powder and $CeCl_3$ (1 mL, 50 mM) aqueous solution are mixed in acetonitrile solution (5 mL). This mixture is then stirred at 600 rpm at room temperature for 6 hours to ensure uniform distribution of Pt and Ce ions. After fully stirred, the mixed solution is transferred to a blast drying oven at 60 ℃ for 12 hours to completely oxidize Ce ions and form the Pt-CeO_2/C heterogeneous catalyst.

3. Synthesis of PtCe-CeO_2/C heterogeneous catalyst

The PtCe-CeO_2/C heterogeneous catalyst was synthesized using the thermal reduction method on the basis of Pt-CeO_2/C heterogeneous catalyst. The Pt-CeO_2/C powder is positioned in a porcelain boat and then heated at 800 °C in a 10% H_2/Ar atmosphere for 4 hours to facilitate the formation of the PtCe alloy. After the thermal processing, the powder is treated with a 0.1 M $HClO_4$ solution to remove surface impurities, followed by three deionized water washes, and concludes with vacuum drying.

4. Materials characterizations

A range of characterization techniques were utilized to determine the chemical properties and structural composition of the catalysts. The crystal structure analysis of PtCe-CeO_2/C, Pt-CeO_2/C and commercial Pt/C catalysts was performed on the powder X-ray diffractometer (XRD) Rigaku SmartLab SE instrument with Cu Kα radiation. The X-ray photoelectron spectroscopy (XPS) was conducted at a Shimadzu/Kratos AXIS SUPRA+ spectroscopy to analyze the surface chemical states of the catalysts. Transmission electron microscope (TEM), high-resolution TEM (HRTEM), and high-angle annular dark-field scanning TEM (HAADF-STEM) images and selected area electron diffraction (SAED) patterns were captured using the JEOL JEM-F200 instrument with an accelerated voltage of 200 kV. The corresponding energy-dispersive X-ray spectra (EDS) were examined on the UPR spectrometer. The proportion of Pt and Ce elements in the PtCe-CeO_2/C and Pt-CeO_2/C catalyst was analyzed by an Agilent 5110 inductively coupled plasma-optical emission spectrometer (ICP-OES).

5. Electrochemical measurements

Electrochemical tests were performed on the CHI 660E workstation using a typical three-electrode system with Pt wire as the counter electrode and Ag/AgCl (3 M KCl) electrode as the reference electrode. Before the catalyst is modified on the glassy carbon electrode (GCE) or rotating disk electrode (RDE), the electrodes are polished with Al_2O_3 powder and then cleaned three times with deionized water and ethanol to remove surface contaminants. All potential measurements referenced to the Ag/AgCl electrode are calibrated to the reversible hydrogen electrode (RHE) by the equation:

$$E_{RHE} = E_{Potential} + E_{Ag/AgCl} + 0.0591 \times pH \#(1)$$

The catalyst ink was prepared by dispersing catalyst powder in a mixture solution containing deionized water, isopropyl alcohol, and 5% Nafion solution with the volume ratio of 150:50:1.

Cyclic voltammetry (CV) measurements were tested in the potential range of 0.0 to 1.2 V (vs RHE) in N_2-saturated 0.5 M H_2SO_4 solution at a scan rate of 50 mV s^{-1}. The electrochemical active surface areas (ECSAs) of the catalysts were evaluated

according to the underpotential deposition behavior of hydrogen which was calculated by the following equation:

$$ECSA = Q_H/0.21[Pt]\#(2)$$

where Q_H was the charge associated with hydrogen desorption, 0.21 mC cm^{-2} was the electrical charge associated with monolayer adsorption of hydrogen on Pt surface, and $[Pt]$ was the mass of Pt loading on the working electrode.

The CO stripping voltammetry was performed in 1.0 M KOH solution. After purging the solution with ultrapure N_2 for 30 min, gaseous CO was bubbled for 30 min to promote the formation of a perfect CO adlayer on the surface of the electrocatalysts. Excess CO traces from the solution as well as the surface of the electrocatalysts were flushed out by purging the solution with ultrapure N_2 for 30 min. The CO stripping voltammetry patterns were recorded under a potential of 0.04-1.34 V vs. RHE at a scan rate of 50 mV s^{-1}.

For MOR measurement, the Pt loading of PtCe-CeO_2/C, Pt-CeO_2/C and commercial Pt/C catalysts on GCE for MOR were controlled at 14.1, 13.8 and 17.9 μg_{Pt} cm^{-2}, respectively. The CV curves were conducted within the potential range of 0.237-1.237 V (vs RHE) with a scan rate of 50 mV s^{-1} in a 1 M KOH solution containing 1 M methanol. The electrochemical impedance spectroscopy (EIS) was tested under the potential of 0.737 V (vs RHE), with the frequency range spanning from 10 kHz to 1 Hz and the amplitude of 5 mV.

For ORR measurement, the Pt loading of PtCe-CeO_2/C, Pt-CeO_2/C and commercial Pt/C catalysts on RDE for ORR were controlled at 20.4, 19.9 and 25.9 μg_{Pt} cm^{-2}, respectively. The linear sweep voltammetry (LSV) curves were obtained by RDE in O_2-saturated 0.1 M KOH electrolyte with a rotation rate of 1600 rpm at a scan rate of 10 mV s^{-1}. The LSV curves for all measurements were iR-corrected on the CHI 660E workstation. The performance of the ORR was evaluated using the kinetic current (J_K) from the equation:

$$J_K = J \times J_L/(J_L - J)\#(3)$$

Polarization curves at different speeds of 400, 625, 900, 1225, 1600, 2025, and 2500 rpm were recorded to calculate the number of transferred electrons. The electron transfer number was evaluated using the Koutecky-Levich equation:

$$\frac{1}{J}=\frac{1}{J_K}+\frac{1}{J_L}=\frac{1}{J_K}+\frac{1}{B\omega^{1/2}}\#(4)$$

$$B=0.2\,nFC_0D_0^{2/3}V^{-1/6}\#(5)$$

where J and J_K are the current density and the kinetic current density. J_L is the diffusion-limiting current density. ω represents the electrode rotation rate (rpm). n is the electron transfer number. F is the Faraday constant (F = 96485 C mol^{-1}). C_0 is the bulk concentration of O_2 (C_0 = 1.26 × 10^{-6} mol cm^{-3}). D_0 is the diffusion coefficient of O_2 in 0.1 M KOH (D_0 = 1.9 × 10^{-5} cm^2 s^{-1}). V is the kinematic viscosity of the electrolyte (V = 1.09 × 10^{-2} cm^2 s^{-1} in 0.1 M KOH).

The H_2O_2 yield (H_2O_2%) and electron transfer number (n) were calculated by the following equations:

$$H_2O_2\%=200\times\frac{I_R/N}{I_D+I_R/N}\#(6)$$

$$n=4\times\frac{I_D}{I_D+I_R/N}\#(7)$$

where I_R is ring current and I_D is disk current. N is the collection efficiency of the ring electrode (0.37 in this work).

6. Performance of DMFCs full cell

The PtCe-CeO_2/C heterogeneous catalyst was applied to the anode and cathode of DMFCs as a bifunctional catalyst, and with the commercial Pt/C catalyst for comparison. Hydrophilic carbon paper is used in the anode chamber to promote the adsorption of substrate methanol, and hydrophobic carbon paper is used in the cathode chamber to quickly remove water. Before the catalyst is modified onto carbon paper, the catalyst powder, deionized water, isopropyl alcohol and ionomer are ultrasonically mixed for 1 hour. The loading amount of anode and cathode catalyst is controlled at 0.3 and 0.2 mg_{Pt} cm^{-2}, respectively. Before testing, the anion exchange membrane Fumasep FAA-3-50 was soaked with 0.5 M NaCl and 1 M KOH solution for 24 hours, respectively. The effective area of a single cell in MEA is 2.0 cm × 2.0 cm (4.0 cm^2).

The steady-state MEA polarization curves of the PtCe-CeO_2/C heterogeneous catalyst and Pt/C at different temperatures and oxygen flow rates were recorded to compare the performance differences. Additionally, the relationship between the voltage and time of different catalysts at a fixed current density of 10 mA cm^{-2} was recorded to compare the durability of different catalysts in DMFCs.

7. Density functional theory calculations

Density functional theory (DFT) calculations were performed via the Vienna ab initio simulation package (VASP).[1] The ion-electron interaction was described with the projector-augmented plane-wave (PAW) method.[2] Exchange-correlation energy was expressed by the Perdew-Burke-Ernzerhof (PBE) functional with the generalized gradient approximation (GGA).[3] It is difficult for DFT to accurately represent the nature of the 4f orbital of cerium, so we executed the DFT+U method which introduced an on-site Coulombic interaction (U term) that penalized non-integer occupation of localized orbitals, effectively penalizing delocalization of electrons.[4] The U value for Ce was 5.0 eV. The Pt-CeO_2 and the PtCe-CeO_2 were simulated by constructing the composite structures of Pt (111) plane and PtCe (111) plane with CeO_2 (111) plane, respectively. To avoid interlayer interaction the vacuum layer was set to be 15 Å. For geometry optimization, the cut-off energy was set to 400 eV and the Brillouin zone was sampled with Monkhorst-Pack 2 × 2 × 1 k-points mesh.[5] The convergence criteria of total energy for electron self-consistent field and force for geometry optimizations were 10^{-5} eV and -0.02 eV $Å^{-1}$, respectively.

According to the computational hydrogen electrode (CHE) model proposed by Nørskov and co-workers,[6] the free energy of the proton-electron pair is equal to that of 1/2 H_2(g). The free energy change for each fundamental step was determined by:

$$\Delta G = \Delta E + \Delta E_{ZPE} - T\Delta S \#(8)$$

Where ΔE is the difference of electronic energy obtained directly from DFT simulation. ΔE_{ZPE} is the difference of variation of zero-point energy (*ZPE*), ΔS is the difference of entropy (*S*) change, and *T* is the temperature (*T* = 298.15K). The *ZPE* and *S* of ORR intermediates were obtained from the vibrational frequencies.

Supporting figures and tables

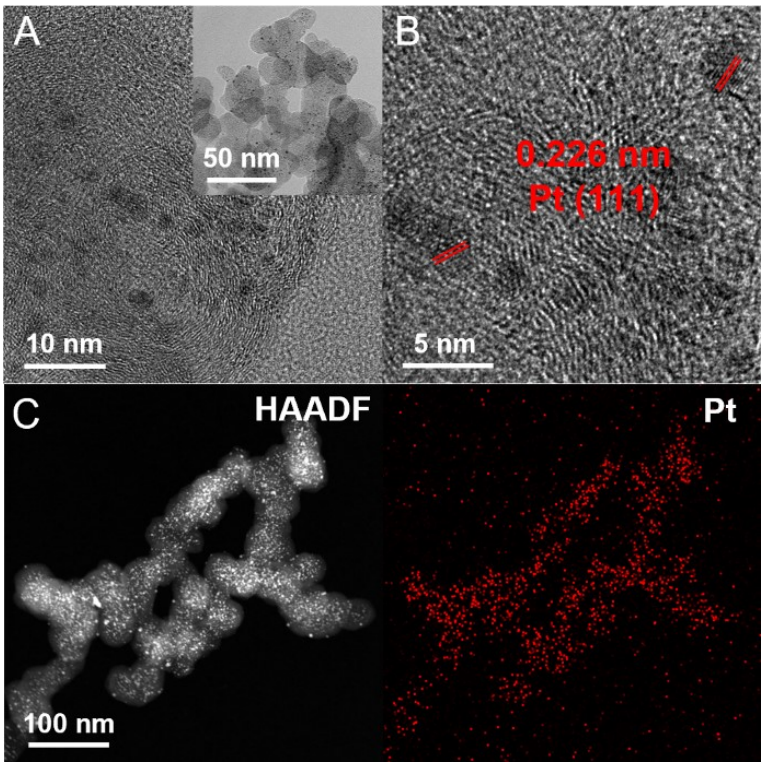

Figure S1. (A) TEM images with different amplifications, (B) HRTEM image for commercial Pt/C catalyst, (C) HADDF-STEM image and corresponding elemental mapping images of Pt.

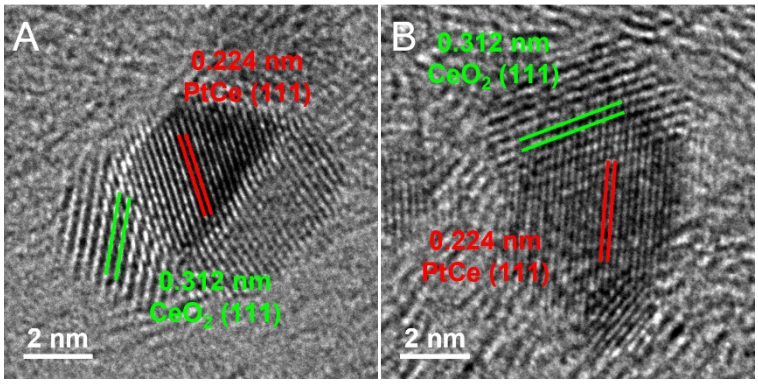

Figure S2. (A, B) HRTEM images of PtCe-CeO_2/C catalyst.

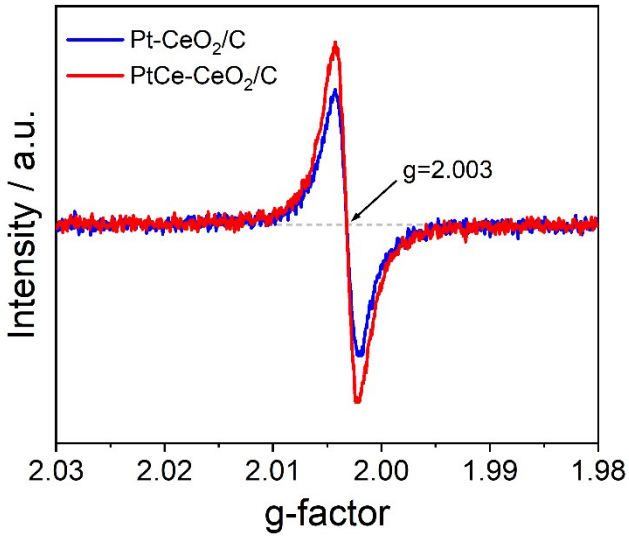

Figure S3. EPR spectra of Pt-CeO_2/C and PtCe-CeO_2/C.

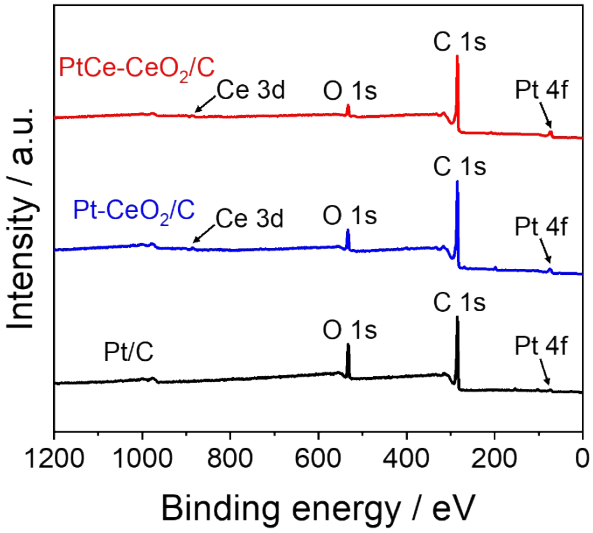

Figure S4. XPS full spectra for PtCe-CeO_2/C, Pt-CeO_2/C and Pt/C catalysts.

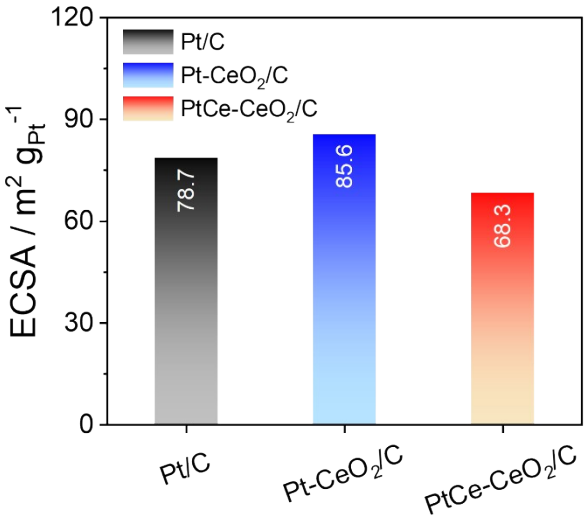

Figure S5. Histogram of ECSAs for Pt/C, Pt-CeO_2/C and PtCe-CeO_2/C catalysts.

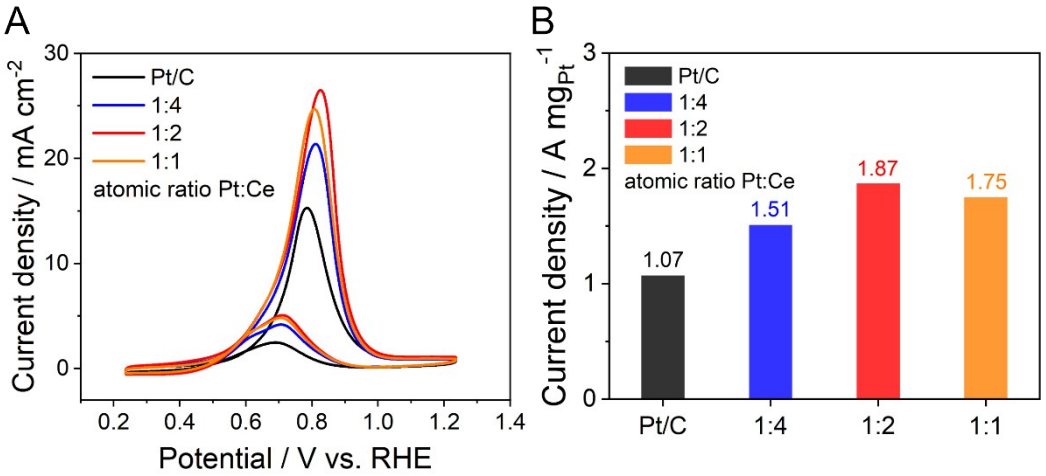

Figure S6. (A) CV curves for electrocatalytic MOR in 1.0 M KOH and 1.0 M CH_3OH solution. (B) Mass activity for Pt/C and Pt-CeO_2/C catalysts with different Pt: Ce feed ratios.

Notes: The influence of different Pt: Ce ratio on MOR performance of catalyst was investigated, and the optimal ratio was Pt: Ce = 1:2 (named as Pt-CeO_2/C in this work, and the subsequent alloying study was also based on this ratio).

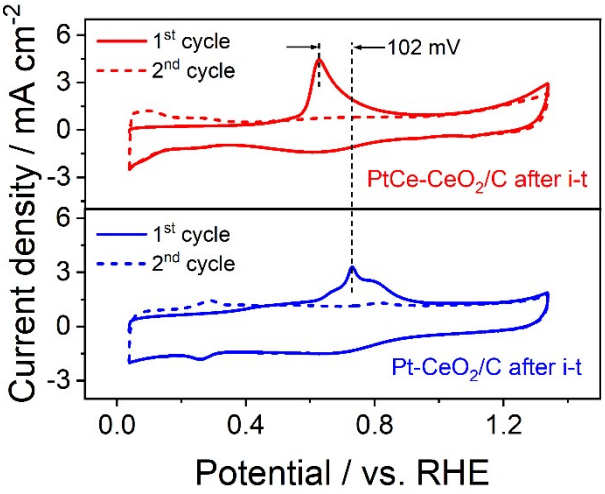

Figure S7 CO stripping voltammograms in 1.0 M KOH solution for Pt-CeO_2/C and PtCe-CeO_2/C catalysts after stability test.

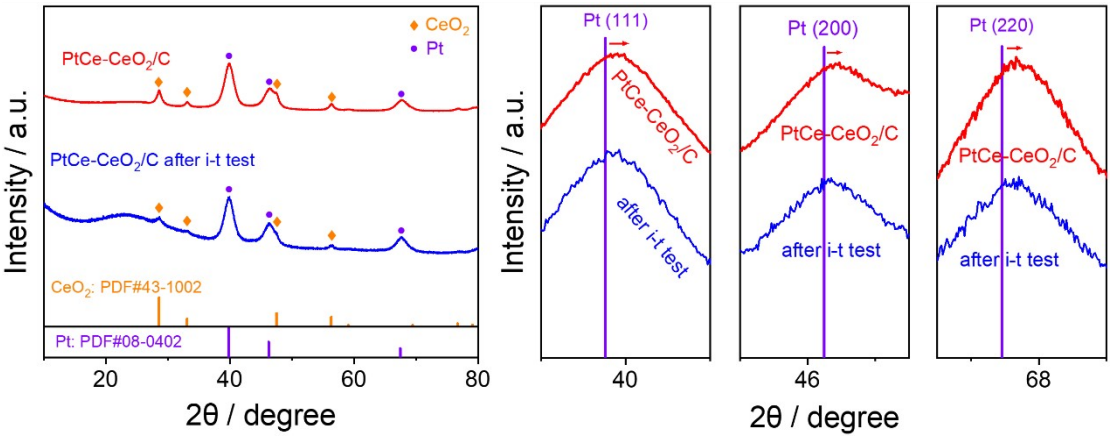

Figure S8 XRD patterns and the enlarged images for PtCe-CeO_2/C sample before and after MOR stability test.

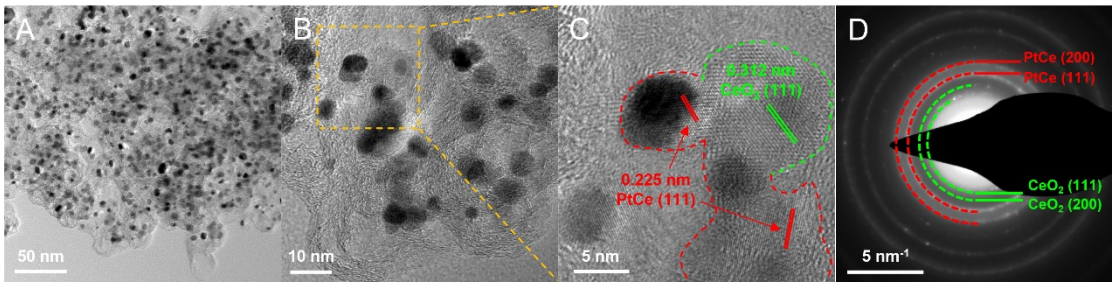

Figure S9 (A, B) TEM images with different amplifications, (C) HRTEM images, (D) SAED pattern for the PtCe-CeO_2/C catalyst after MOR stability test.

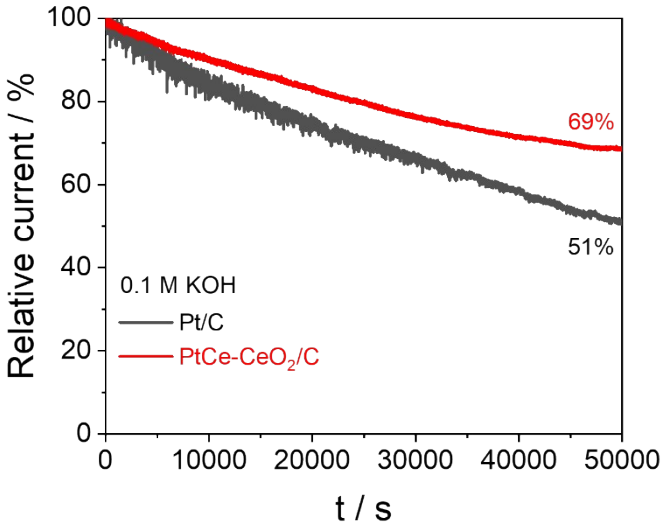

Figure S10. Stability tests for Pt/C and PtCe-CeO_2/C catalysts in O_2-saturated 0.1 M KOH solution.

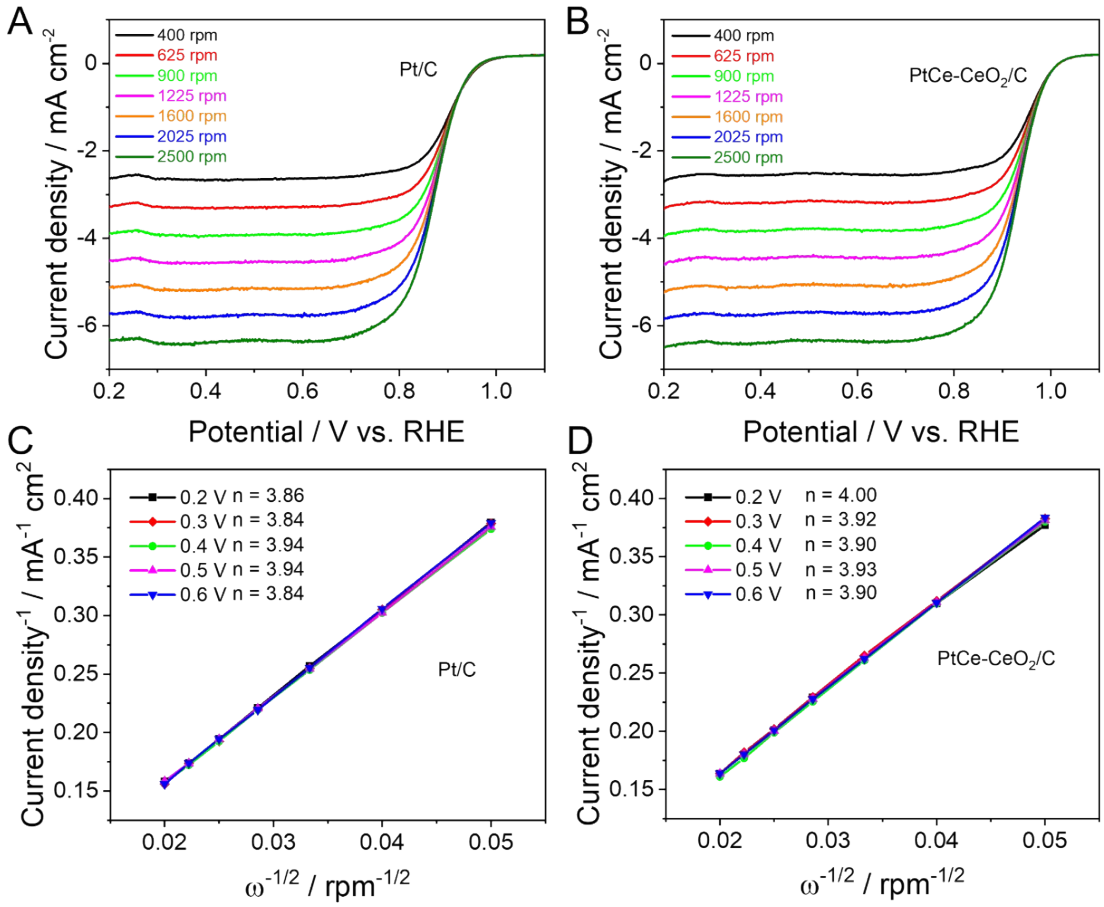

Figure S11. (A, B) LSV curves of Pt/C and PtCe-CeO_2/C catalysts in O_2-saturated 0.1 M KOH solution at different rotation speeds. (C, D) The Koutecky-Levich plots of Pt/C and PtCe-CeO_2/C catalysts for ORR at different potentials.

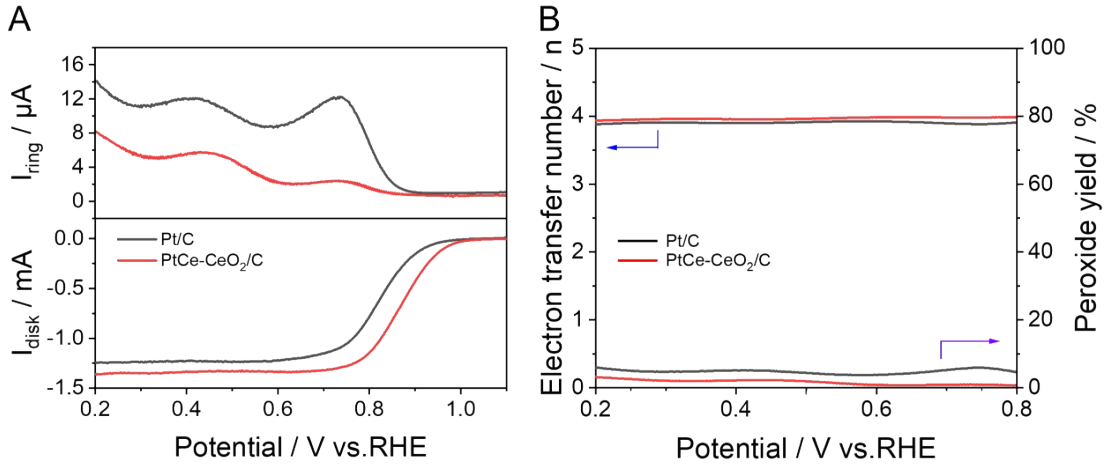

Figure S12. (A) Typical RRDE polarization curves of the Pt/C and PtCe-CeO_2/C catalysts. (B) Electron-transfer number and H_2O_2 yield for Pt/C and PtCe-CeO_2/C catalysts.

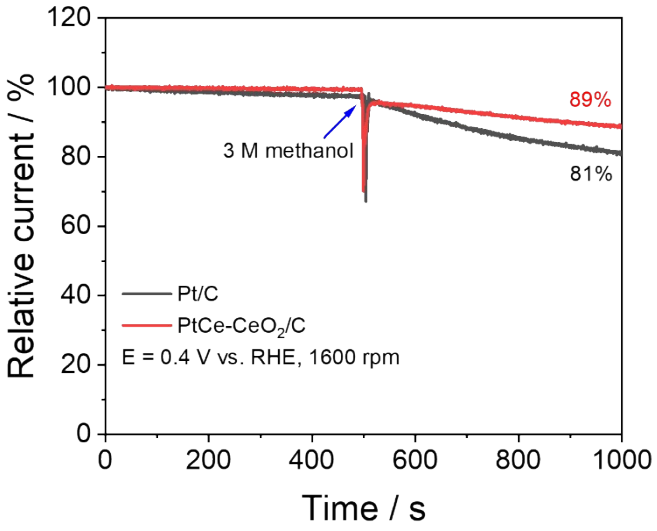

Figure S13. Methanol tolerance test of Pt/C and PtCe-CeO_2/C at 0.4 V vs. RHE with a rotation rate of 1600 rpm in 0.1 M KOH solution.

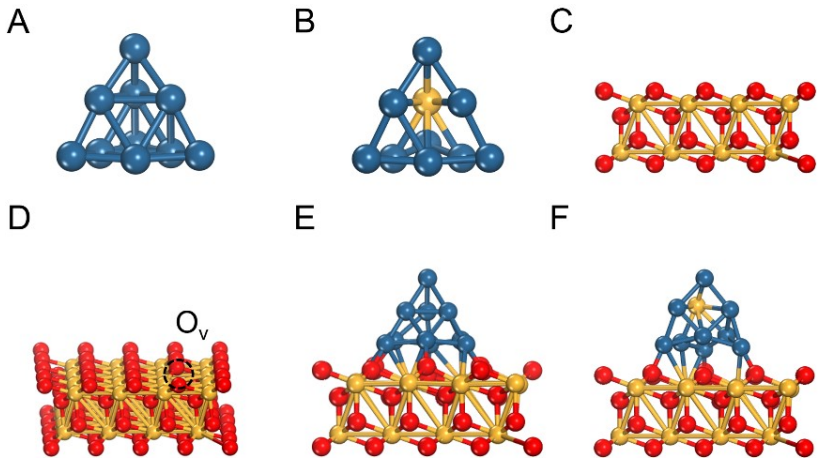

Figure S14. Model structures of (A) Pt (111) cluster; (B) PtCe (111) cluster; (C, D) CeO_2 (111)-O_v; (E) Pt-CeO_2 and (F) PtCe-CeO_2.

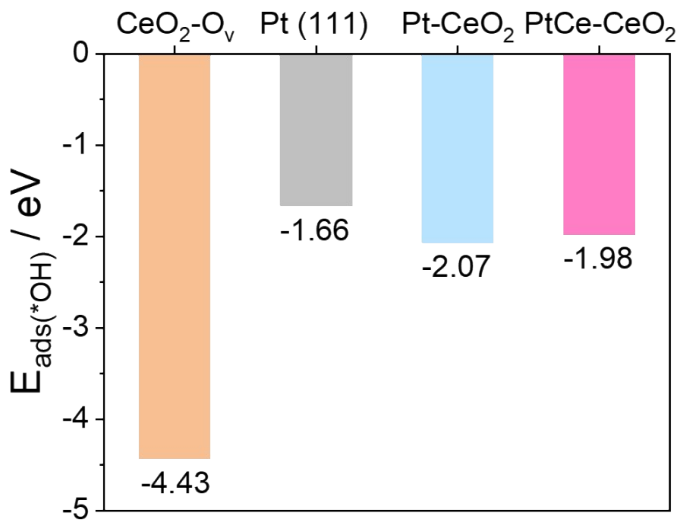

Figure S15. Adsorption energy of *OH on CeO_2-O_v, Pt (111), Pt-CeO_2 and PtCe-CeO_2.

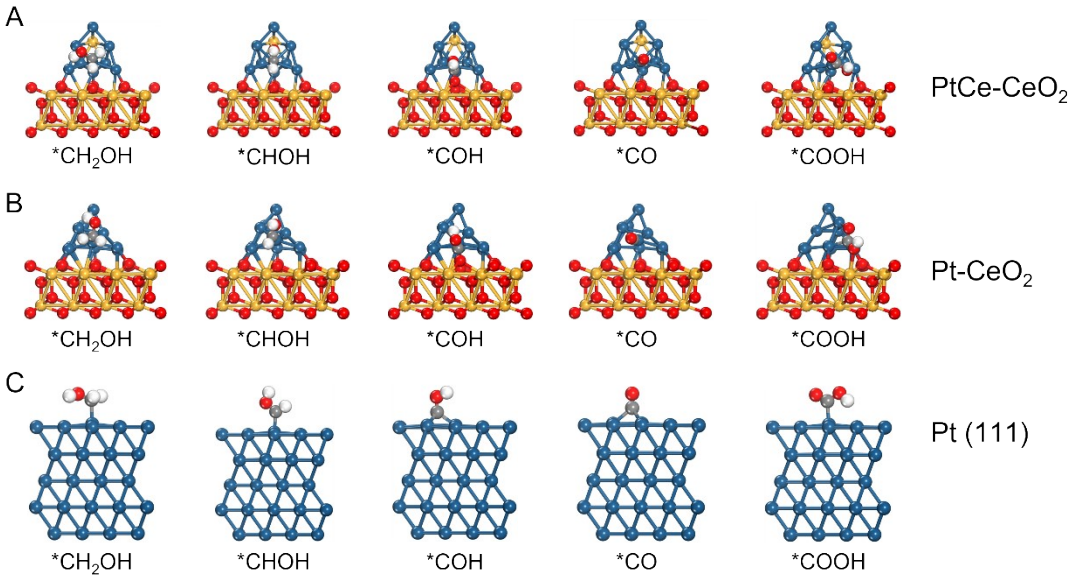

Figure S16. Model structures of *CH_2OH, *CHOH, *COH, *CO, *COOH adsorbed on (A) PtCe-CeO_2; (B) Pt-CeO_2 and (C) Pt (111).

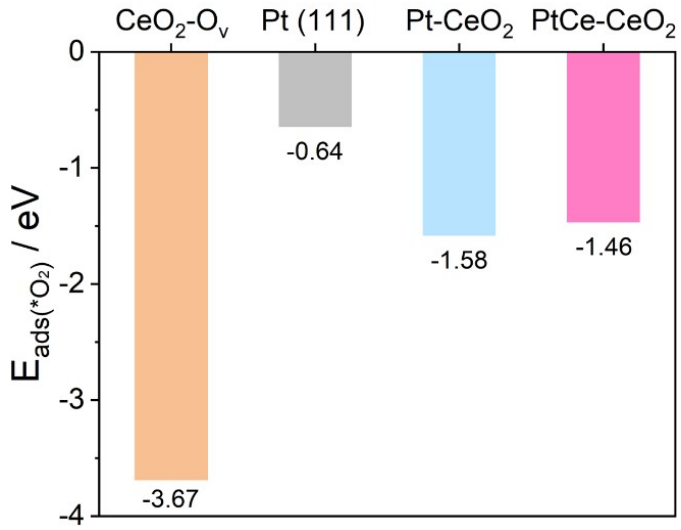

Figure S17. Adsorption energy of O_2 on CeO_2-O_v, Pt (111), Pt-CeO_2 and PtCe-CeO_2.

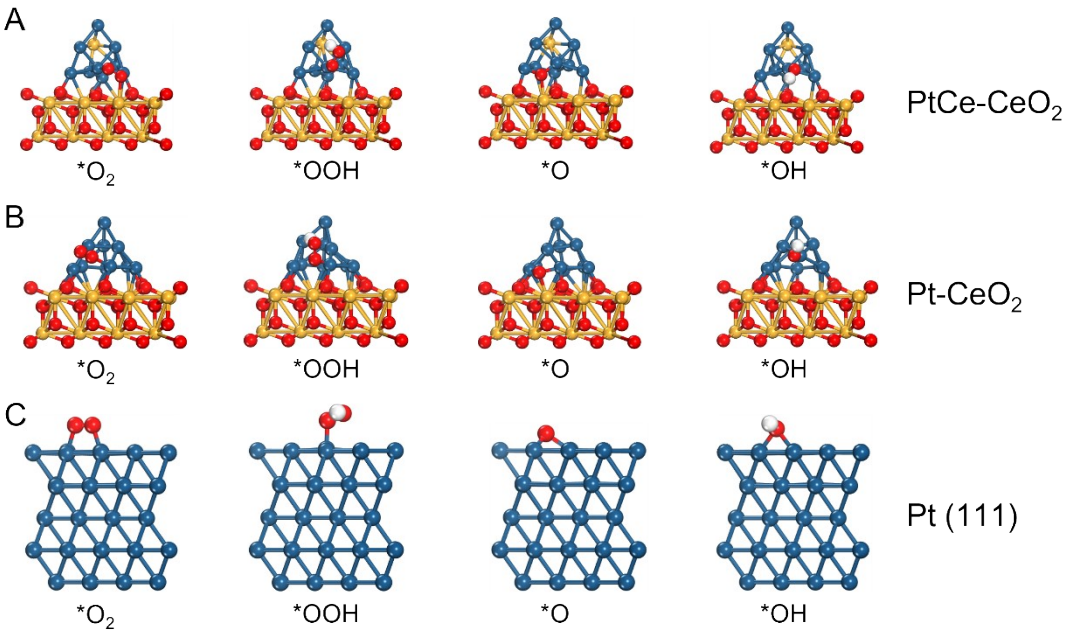

Figure S18. Model structures of $*O_2$, *OOH, *O and *OH adsorbed on (A) PtCe-CeO_2, (B) Pt-CeO_2 and (C) Pt (111).

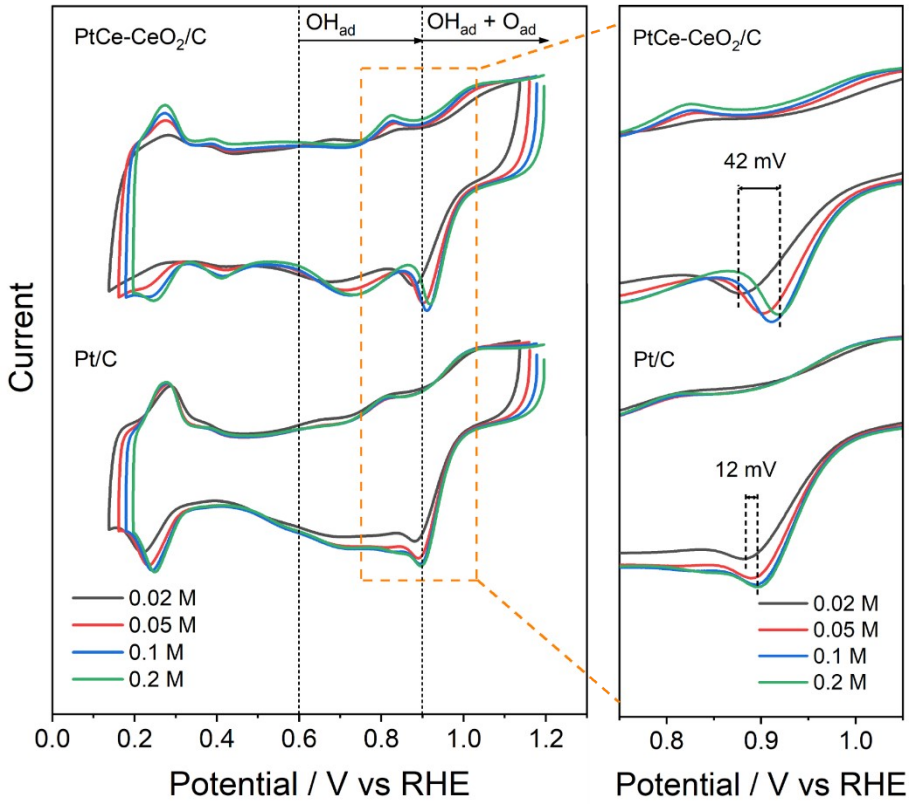

Figure S19. CV curves of PtCe-CeO_2/C and Pt/C catalysts in O_2-saturated KOH solutions with different concentrations.

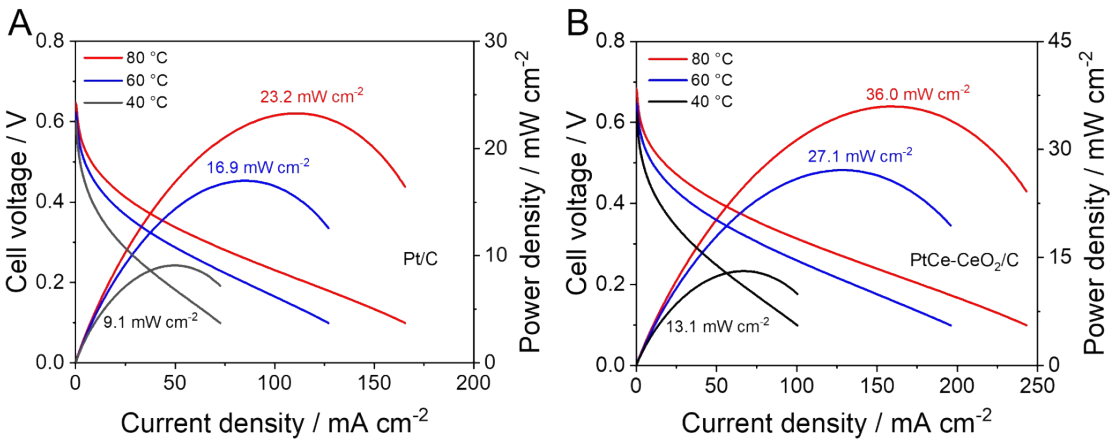

Figure S20. Polarization curves of DMFCs at different temperature for (A) Pt/C and (B) PtCe-CeO_2/C catalysts.

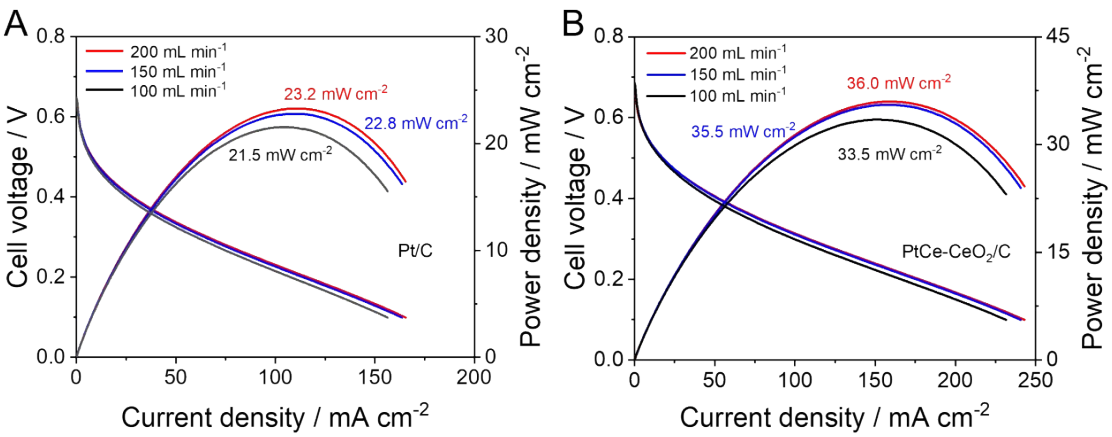

Figure S21. Polarization curves of DMFCs at different O_2 flow rates for (A) Pt/C and (B) PtCe-CeO_2/C catalysts, temperature: 80 °C.

Table S1. The content of different Pt species in Pt/C, Pt-CeO_2/C and PtCe-CeO_2/C samples.

Samples	Pt(0)	Pt(II)
Pt/C	60.46%	39.54%
Pt-CeO_2/C	59.29%	40.71%
PtCe-CeO_2/C	69.19%	30.81%

Table S2. The content of different Ce species in Pt-CeO_2/C and PtCe-CeO_2/C samples.

Samples	Ce(III)	Ce(IV)
Pt-CeO_2/C	43.01%	56.99%
PtCe-CeO_2/C	33.69%	66.31%

Table S3. Fitting data details of the Nyquist plots for Pt/C, Pt-CeO_2/C, PtCe-CeO_2/C and PtRu/C catalysts in MOR.

Catalysts	R_{ct} / Ω	R_s / Ω	CPE-T / $S \cdot s^n \cdot cm^{-2}$	CPE-P
Pt/C	143.4	11.5	0.00023	0.989
Pt-CeO_2/C	114.9	15.2	0.00036	0.960
PtCe-CeO_2/C	88.2	13.2	0.00025	0.984
PtRu/C	144.2	10.3	0.00023	0.928

Table S4. ORR performance of Pt/C, Pt-CeO_2/C and PtCe-CeO_2/C catalysts in O_2-saturated 0.1 M KOH.

Catalysts	Onset potential / V vs RHE	$E_{1/2}$ / V vs RHE	J_K (@0.9 V vs RHE) / A mg_{Pt}^{-1}	Mass activity / A mg_{Pt}^{-1}	Specific activity / mA cm_{Pt}^{-2}
Pt/C	0.967	0.874	2.369	0.116	0.148
Pt-CeO_2/C	0.983	0.904	4.965	0.250	0.292
PtCe-CeO_2/C	1.010	0.946	28.215	1.090	1.596

Table S5. MEA performance of DMFCs for Pt/C and PtCe-CeO_2/C catalysts at different temperature.

Catalyst	Temperature / ℃	OCV / V	Maximum power density / mW cm^{-2}
Pt/C	40	0.600	9.1
	60	0.622	16.9
	80	0.646	23.2
PtCe-CeO_2/C	40	0.624	13.1
	60	0.646	27.1
	80	0.682	36.0

Table S6. Fitting data details of the Nyquist plots for Pt/C, and PtCe-CeO_2/C catalysts in DMFCs.

Catalysts	R_{ct} / Ω	R_s / Ω	CPE-T / $S \cdot s^n \cdot cm^{-2}$	CPE-P
Pt/C	2.83	0.38	0.126	0.745
PtCe-CeO_2/C	1.29	0.36	0.137	0.739

Table S7. The comparison of parameters of noble metal catalysts in DMFCs.

Anode catalysts	Loading at anode (mg_{NM} cm^{-2})	Cathode catalysts	Loading at cathode (mg_{NM} cm^{-2})	Electrolyte	Peak power density (mW cm^{-2})	Mass power density (mW mg_{Pt}^{-1})
PtCe-CeO_2/C (this work)	0.3	PtCe-CeO_2/C	0.2	1 M KOH + 1 M CH_3OH	36.0 (low noble metal loading)	72.0
SE-Bi_1/Pt NRs [7]	0.39	Pd/C	1.35	6 M KOH + 4 M CH_3OH	85.3	49.0
$PdSn_{0.5}$/Se-Ti_3C_2 [8]	0.5	Pt/C	0.5	3 M NaOH + 1 M CH_3OH	10.2	10.2
PtCu NWs [9]	0.6	Pt/C	2	/ + 1 M CH_3OH	49.7	19.1
PtRu/C [10]	2.4	Pt/NC	2	0.1 M $HClO_4$ + 4 M CH_3OH	25.9	5.9
PtRu/C [11]	2	Acta 4020	3	6 M KOH + 3 M CH_3OH	305	61
PtRu/C [12]	3.5	Pt/C	1.75	6 M KOH + 4 M CH_3OH	87.8	16.7
PtRu/C [13]	4	3D GF + Pt/C	2	/ + 3 M CH_3OH	25.7	6
Pd-PdO PNTs [14]	4	Pt/C	4	1 M KOH + 5 M CH_3OH	6.2	0.8

Reference

[1] G. Kresse and J. Furthmüller, Efficiency of ab-initio total energy calculations for metals and semiconductors using a plane-wave basis set, *Comp. Mater. Sci.*, 1996, **6**, 15-50.

[2] P. Blöchl, Projector augmented-wave method, *Phys. Rev. B*, 1994, **50**, 17953.

[3] J. Perdew, K. Burke and M. Ernzerhof, Generalized gradient approximation made simple, *Phys. Rev. Lett.*, 1996, **77**, 3865.

[4] S. Fabris, S. Gironcoli, S. Baroni, G. Vicario and G. Balducci, Taming multiple valency with density functionals: A case study of defective ceria, *Phys. Rev. B*, 2005, **71**, 041102.

[5] H. Monkhorst and J. D. Pack, Special points for Brillouin-zone intergrations, *Phys. Rev. B*, 1976, **13**, 5188-5192.

[6] J. Nørskov, J. Rossmeisl, A. Logadottir, L. Lindqvist, J.R. Kitchin, T. Bligaard and H. Jónsson, Origin of the overpotential for oxygen reduction at a fuel-cell cathode, *J. Phys. Chem. B*, 2004, **108**, 17886-17892.

[7] X. Fan, W. Chen, L. Xie, X. Liu, Y. Ding, L. Zhang, M. Tang, Y. Liao, Q. Yang, X. Fu, S. Luo and J. Luo, Surface-enriched single-Bi-atoms tailoring of Pt nanorings for direct methanol fuel cells with ultralow-Pt-loading, *Adv. Mater.*, 2024, **36**, 2313179.

[8] S. Chen, N. Liu, J. Zhong, R. Yang, B. Yan, L. Gan, P. Yu, X. Gui, H. Yang, D. Yu, Z. Zeng and G. Yang, Engineering support and distribution of Palladium and Tin on MXene with modulation of the d-band center for CO-resilient methanol oxidation, *Angew. Chem. Int. Ed.*, 2022, **61**, e202209693.

[9] K. Wang, D. Huang, Y. Guan, F. Liu, J. He and Y. Ding, Fine-tuning the electronic structure of dealloyed PtCu nanowires for efficient methanol oxidation reaction, *ACS Catal.*, 2021, **11**, 14428-14438.

[10] Y. Zhang, W. Yuan, C. Hou, Y. Li, S. Liu, C. Deng, F. Ji, Y. Zhang and X. Zhang, Improved DMFC water management via superwetting, high-performance catalyst synthesized by nanocapsule method, *Appl. Surf. Sci.*, 2024, **644**, 158756.

[11] M. Wu, X. Zhang, Y. Zhao, C. Yang, S. Jing, Q. Wu, A. Brozena, J. Miller, N. Libretto, T. Wu, S. Bhattacharyya, M. Garaga, Y. Zhang, Y. Qi, S. Greenbaum, R. Briber, Y. Yan and L. Hu, A high-performance hydroxide exchange membrane enabled by Cu^{2+}-crosslinked chitosan, *Nat. Nanotechnol.*, 2022, **17**, 629-636.

[12] Y. Zhang, B. Huang, G. Luo, T. Sun, Y. Feng, Y. Wang, Y. Ma, Q. Shao, Y. Li, Z. Zhou and X. Huang, Atomically deviated Pd-Te nanoplates boost methanol-tolerant fuel cells, *Sci. Adv.*, 2020, **6**, eaba9731.

[13] W. Yuan, X. Zhang, C. Hou, Y. Zhang, H. Wang and X. Liu, Enhanced water management via the optimization of cathode microporous layer using 3D graphene frameworks for direct methanol fuel cell, *J. Power Sources*, 2020, **451**, 227800.

[14] T. Wang, F. Li, H. Huang, S. Yin, P. Chen, P. Jin and Y. Chen, Porous Pd-PdO nanotubes for methanol electrooxidation, *Adv. Funct. Mater.*, 2020, **30**, 2000534.